# Condensation of a Nickel Tetranuclear Cubane into a Heptanuclear Single-Molecule Magnet

Sarah Petit,[†] Petr Neugebauer,[‡] Guillaume Pilet,[†] Guillaume Chastanet,[†,‖] Anne-Laure Barra,[‡] Arlei B. Antunes,[‡] Wolfgang Wernsdorfer,[§] and Dominique Luneau*,[†]

[†]Laboratoire des Multimatériaux et Interfaces (UMR 5615), Université Claude Bernard Lyon 1, Campus de la Doua, 69622 Villeurbanne Cedex, France

[‡]Laboratoire National des Champs Magnétiques Intenses-CNRS, Université Joseph Fourier, 25 Avenue des Martyrs, 38042 Grenoble Cedex 9, France

[§]Institut Néel-CNRS, BP166, 25 Avenue des Martyrs, 38042 Grenoble Cedex 9, France

**Ⓢ** *Supporting Information*

**ABSTRACT:** A tetranuclear complex, [**Ni₄**], with a cubane-like structure synthesized from hexafluoroacetylacetone gives, after drying at high temperature and treatment with pyridine, a heptanuclear nickel(II) complex, [**Ni₇**]. The crystal structures of both compounds have been determined by single-crystal X-ray diffraction. Their magnetic properties have been studied by SQUID and $\mu$-SQUID magnetometry as well as by high-frequency EPR spectroscopy (HF-EPR). For [**Ni₄**], the temperature dependence of the magnetic susceptibility can be fitted by taking into account strong Ni···Ni ferromagnetic interactions which lead to an $S = 4$ ground-state spin, in good agreement with the HF-EPR study. For [**Ni₇**], the temperature dependence of the magnetic susceptibility shows that the Ni···Ni ferromagnetic interactions are kept within the metal core. However, it was not possible to fit this with a clear set of parameters, and the ground-state spin was undetermined. The field dependence of the magnetization indicates an $S = 7$ ground-state spin at high field. In contrast, the temperature dependence of the magnetic susceptibility indicates a ground-state spin of $S = 6$ or even $S = 5$. These results agree with complicated high-frequency EPR spectra which have been ascribed to the superposition of signals from the ground spin multiplet and from an excited spin multiplet very close in energy, with the excited state having a larger $S$ value than the ground state. Very low temperature studies show that only the heptanuclear complex behaves as a single-molecule magnet.
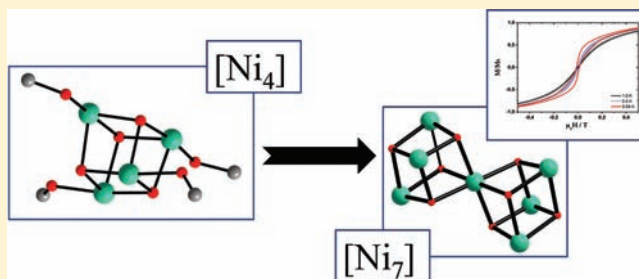
## INTRODUCTION

The design of superparamagnetic clusters known as single-molecule magnets (SMMs)[1–5] has currently given rise to a considerable amount of work.[6–8] The ability of these molecules to be magnetized and to relax very slowly below a blocking temperature has led to important breakthroughs in the study of nanosize magnetic systems and may find potential applications in information processing.[9,10] The prerequisite for such a molecular magnetic memory is the combination of a high-spin ground-state value ($S$) and of magnetic anisotropy with large negative zero-field splitting ($D < 0$).[11,12] Consequently, most efforts devoted to the chemical design of SMMs have concentrated on the synthesis of large clusters with both high spin and uniaxial magnetic anisotropy, as exemplified by different strategies.[8,13–19]

As part of our investigations on polynuclear systems exhibiting SMM properties, we have been interested in cubane-like structures as molecular bricks to build systems with high nuclearity. Indeed, their particular geometrical arrangement generally favors ferromagnetic interactions and

thus molecules with high-spin ground states.[20–26] For decades, magneto-structural studies have discussed the role of the cubane geometry in the exchange interaction[27–29] as well as in the anisotropy.[24,30–32] Thus, we previously reported on the synthesis and magnetic properties of lanthanide–copper systems with controlled tetra ([Cu₃Ln])- and nonanuclearities ([Cu₆Ln₃]).[33] They were synthesized by starting from the tetranuclear copper(II) complex [Cu₄] with a cubane-like structure,[34] and the magnetic study of the nonanuclear [Dy₃Cu₆] revealed SMM behavior.[33] We also investigated the magneto-structural relationships of this tetranuclear copper(II) complex [Cu₄] by polarized neutron diffraction.[35] Among these studies, we also reported on a [Co$^{II}_3$Co$^{III}_4$] mixed-valence heptanuclear complex made up of two cubane moieties, for which we explained the lack of SMM behavior by a theoretical study.[36]

In the present paper we report on the use of a tetranuclear complex $[\mathbf{Ni_4}]$ (**1**) with a cubane-like structure as a molecular building block from which we succeeded in generating, by a condensation-like process, the new heptanuclear nickel(II) complex $[\mathbf{Ni_7}]$ (**2**), which can be viewed as two cubes sharing one metal corner. The molecular structures of these systems, $[\mathbf{Ni_4}]$ (**1**) and $[\mathbf{Ni_7}]$ (**2**), have been elucidated and their magnetic properties studied by SQUID and $\mu$-SQUID magnetometry as well as by high-field and high-frequency EPR spectroscopy (HF-EPR). In the case of $[\mathbf{Ni_7}]$ they evidence a SMM behavior. Regarding the field of SMMs, dominated by manganese-based clusters,[1,8,14,37−40] such systems involving nickel ions are uncommon.[41−54] Thus, several $\{Ni_4\}$ cubes with $S = 4$ ground state have been studied and their anisotropy tuned by ligand substitutions.[45,46,49,51−54] Other nickel-based SMMs such as $\{Ni_5\}$ with $S = 5$,[50] $\{Ni_8\}$ with $S = 8$,[47] $\{Ni_{10}\}$ with $S = 10$,[48] $\{Ni_{12}\}$ with $S = 12$,[41,43] and $\{Ni_{21}\}$ with $S = 3$[44] have been shown to have small anisotropy factors.

## ■ EXPERIMENTAL SECTION

**Syntheses.** All chemicals were used as received.

*[Ni4(hfac)4(CH3OH)4(CH3O)4] (1).* A solution of NaOH (56 mg, 1 mmol) in 20 mL of methanol was added drop by drop to a refluxing solution of $Ni(hfac)_2 \cdot 2H_2O$ in 10 mL of methanol (518 mg, 1 mmol). After additional stirring under reflux over 2 h, the green solution was cooled to room temperature. Suitable crystals for X-ray diffraction were obtained by slow evaporation of the solvent after 2−3 days. Yield: 75%. Anal. Calcd for $C_{28}H_{32}F_{24}Ni_4O_{16}$: C, 25.57; H, 2.45 F, 34.67; Ni, 17.85; O, 19.46. Found: C, 25.43; H, 2.74; Ni, 17.61.

*[Ni7(OH)8(hfac)6(py)6]·py (2·py).* A polycrystalline powder of **1** (657 mg, 0.5 mmol) was placed under vacuum for 1 day in a Schlenk tube. Then, the compound was smoothly heated around 40−50 °C over 1 h, after which changes in color and crystallinity were observed. The resulting powder was dissolved in 5 mL of diethyl ether under a nitrogen atmosphere and stirred for one night. Then 4 mmol of pyridine in 5 mL of diethyl ether was then added drop by drop and the solution stirred for 1 day more. Suitable crystals for X-ray analyses were obtained by very slow evaporation of the solvent. Yield: 30%. Anal. Calcd for $C_{70}H_{54}F_{36}N_8Ni_7O_{20}$: C, 34.71; H, 2.25; F, 28.24; N, 4.63; Ni, 16.96; O, 13.21. Found (%): C, 34.52; H, 2.33; N, 4.35; Ni, 16.87.

**Single-Crystal X-ray Diffraction.** Diffraction data were collected on a Nonius Kappa CCD and the related software.[55] All structures were solved by direct methods using the SIR97 program[56] combined with Fourier difference synthesis and refined on $F$ within the CRYSTALS program.[57] For each structure, all atomic displacements for non-hydrogen atoms were refined anisotropically. Hydrogen atoms belonging to carbon atoms were located theoretically and the others (belonging to oxygen atoms) by difference Fourier. All hydrogen atoms were then refined keeping some restraints (bond lengths and isotropic atomic displacements).

X-ray crystallographic data and refinement details are summarized in Table 1. Selected interatomic bond lengths, distances, and angles are given in Tables 2 and 3 for **1** and **2**, respectively.

**SQUID Magnetometry.** dc magnetic data were recorded using a Quantum Design SQUID magnetometer. The magnetic susceptibilities were measured from 2 to 300 K on polycrystalline samples with an applied field of 1 kOe. To avoid orientation in the magnetic field, the samples were pressed in a homemade Teflon sample holder equipped with a piston. The magnetization was measured at 2 and 5 K in the 0−100 kOe range. The data were corrected for diamagnetism of the constituent atoms using Pascal's constants.

**Micro-SQUID.** Magnetization measurements on single crystals were also performed with an array of Micro-SQUIDs.[11] This magnetometer works in the temperature range ∼0.04−7 K with applied fields up to 14 kOe. The time resolution was approximately 1

**Table 1. Crystal Data and Structure Refinement Parameters for 1 and 2**

| | $[Ni_4(hfac)_4(MeO)_4(MeOH)_4]$ (1) | $[Ni_7(OH)_8(hfac)_6(py)_6]\cdot py$ (2) |
|---|---|---|
| formula | $C_{28}H_{32}F_{24}Ni_4O_{16}$ | $C_{70}H_{54}F_{36}N_8Ni_7O_{20}$ |
| formula wt | 1315.34 | 2422.02 |
| cryst syst | monoclinic | monoclinic |
| space group | $C2/c$ (No. 15) | $P2_1/n$ (No. 14) |
| $T$ (K) | 293 | 293 |
| $Z$ | 8 | 2 |
| $a$ (Å) | 35.49(3) | 12.705(3) |
| $b$ (Å) | 12.995(4) | 18.75(2) |
| $c$ (Å) | 23.98(1) | 21.701(7) |
| $\beta$ (deg) | 121.66(3) | 91.70(1) |
| $V$ (Å$^3$) | 9414(9) | 5166(5) |
| no. of indep rflns | 11 124 | 10 782 |
| $R_{int}$ | 0.055 | 0.090 |
| $D$ (g cm$^{-3}$) | 1.856 | 1.557 |
| $\mu$ (mm$^{-1}$) | 1.732 | 1.374 |
| $R$ ($I/\sigma(I) > 3$) | 0.0515 | 0.0801$^a$ |
| $R_w$ ($I/\sigma(I) > 3$) | 0.0610 | 0.0884$^a$ |
| $S$ | 1.08 | 1.15 |
| no. of rflns used | 6602 | 4627 |
| no. of refined params | 641 | 663 |
| $\Delta\rho_{max}$ (e Å$^{-3}$) | 2.18 | 0.93 |
| $\Delta\rho_{min}$ (e Å$^{-3}$) | −1.01 | −1.09 |

$^a$In this case, $R_w$ ($I/\sigma(I) > 2$).

ms. The field can be applied in any direction of the Micro-SQUID plane with a precision smaller than 0.1° by separately driving three orthogonal coils. The field was then aligned with the easy axis of magnetization using a transverse field method.[58] The thermalization was guaranteed by the fixation of the single crystals with Apiezon grease.

**EPR Study.** high-field/high-frequency EPR (HF-EPR) spectra were recorded on polycrystalline powder samples, pressed into pellets in order to avoid orientation effects, at three frequencies (190, 230, and 285 GHz) and several temperatures in the range 5−20 K for both compounds. For complex **2**, measurements at 345 GHz were also performed. The HF-EPR spectrometer is a home-built system working in a single-pass configuration. The main magnetic field was supplied by a superconducting magnet with a maximum field of 12 T. The exciting frequencies were generated by phase-locked Gunn diodes operating at either 95 or 115 GHz, equipped with multipliers (doublers or triplers). The transmitted signal was then recorded by a hot electron InSb bolometer. Calculated spectra were produced using the EPR simulation software of Weihe.[59]

## ■ RESULTS AND DISCUSSION

$\beta$-Diketones are well-known for their ability to coordinate metal ions and to generate various polynuclear architectures.[60,61] Their different coordination modes, as well as the wide range of functional groups they can hold, allow tuning the nuclearity and electronic properties of the metal complexes, as we have recently shown with a series of lanthanide clusters.[62] The ability of acetylacetone and its Schiff base derivatives to yield $\{M_4\}$ tetranuclear systems with cubane-like structures that favor ferromagnetic interactions and high ground-state spin has been

known since the 1970s. A Ni(II) cubane cluster with acetylacetone (acac), $[Ni_4(OCH_3)_4(acac)_4(CH_3OH)_4]$, has been shown to exhibit an $S = 4$ ground-state.[20] In previous years, we revisited these works with the notion of using the $\{M_4\}$ cubanes as molecular bricks to get high-nuclearity complexes or extended networks. However, with acetylacetone (acac) the derivatives are sparingly soluble in common solvents, which makes their use as molecular building blocks difficult. This prompted us to use the fluorinated derivative hexafluoroacetylacetone (hfac) instead of acetylacetone. Indeed, the introduction of fluorinated groups favors the solubility of the clusters and their ability to be handled in the reaction. Thus, we previously reported the synthesis and the studies of magneto-structural relationships for several clusters with a Schiff base based on trifluoroacetylacetone along with tetranuclear copper,[35] heptanuclear cobalt(II,III),[36] and tetra- and non-anuclear lanthanide−copper systems.[33,34] Following this route, we synthesized the $[Ni_4(OCH_3)_4(hfac)_4(CH_3OH)_4]$ cluster (**1**) and checked that the $S = 4$ ground state was retained as in the acac derivative.[20] Further, we found that the reaction of **1** with pyridine under dry conditions led to the "condensation" of two cubanes **1** into the novel heptanuclear nickel(II) architecture $[Ni_7(OH)_8(hfac)_6(py)_6]$ (**2**). We note that the apparent "condensation" may be much more complicated from the point of view of the chemical mechanisms. Indeed, the direct synthesis, from nickel salts, of the $[\mathbf{Ni_7}]$ (**2**) cluster was not possible and, despite several trials, the use of the $[\mathbf{Ni_4}]$ (**1**) precursor was necessary. The reactivity of pyridine has already been observed to allow generating clusters of higher nuclearity. For example, a $\{Ni_4\}$ system was synthesized from a mononuclear nickel complex but it decomposed easily to the precursor after the loss of coordinated pyridine.[63] In our case the resulting heptanuclear nickel(II) is found to be stable. Complex **2** is the second nickel-based heptanuclear cluster reported to date.[64]

**X-ray Crystal Structures.** $[Ni_4(OCH_3)_4(hfac)_4(CH_3OH)_4]$ **(1).** The cluster crystallizes in the monoclinic $C2/c$ space group. The asymmetric unit corresponds to the whole cluster and can be described by the four metal ions possessing a tetrahedral arrangement (Figure 1a). Each metal is linked to the others by three of the four deprotonated $\mu_3$-OCH$_3$ molecules (O1, O2, O3, and O4) to form the $\{Ni_4O_4\}$ cubane entity (Figure 1b). The coordination spheres of the Ni(II) ions are completed by two oxygen atoms from one deprotonated hfac ligand and one oxygen atom from one coordinated protonated $\mu$-OHCH$_3$ solvent molecule (Figure 1a). The resulting $[Ni_4(OCH_3)_4(hfac)_4(CH_3OH)_4]$ complex is then neutral with a slightly distorted $\{Ni_4O_4\}$ core, as the Ni−O−Ni and the O−Ni−O angles vary from 95.6 to 98.4° and from 81.4 to 83.6°, respectively (Figure 1b). Moreover, the coordination polyhedron of the Ni(II) is almost a regular octahedron, as the O−Ni−O angles only deviate from 90° by less than 8° and the Ni−O bond lengths vary by less than 0.04 Å around the mean value of 2.06 Å. However, we note that the Ni−OHCH$_3$ bond lengths (2.092 Å) are slightly longer than the other ones. Of the six Ni···Ni distances, four are around 3.057 Å while the two other are around 3.100 Å (Table 2).

The shortest distance between the nickel atoms of two cubane cores is 9.648 Å, while hydrogen bonds are found only within the clusters between coordinated methanol and oxygen atoms of the hfac ligand of the neighboring metal ion. Thus, the structural cohesion is ascribed to weak interactions between the $[Ni_4]$ neutral clusters which are well magnetically isolated.
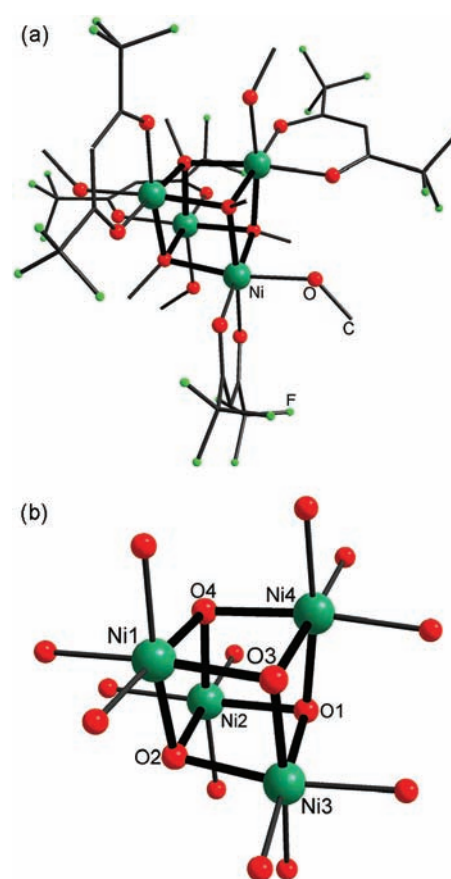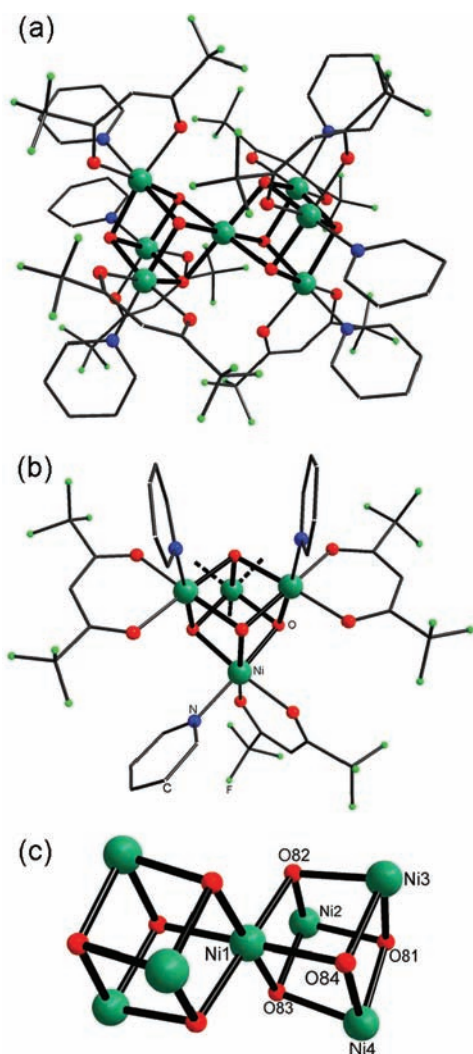


**Figure 1.** (a) Molecular structure of $[\mathbf{Ni_4}]$ (**1**). Hydrogen atoms have been omitted for clarity. (b) View of the $\{Ni_4O_4\}$ cubane core.

**Table 2. Selected Bond Lengths (Å), Distances (Å), and Angles (deg) for 1**

| | | | |
|---|---|---|---|
| Ni1−O2 | 2.045(3) | Ni4−O1 | 2.056(3) |
| Ni1−O3 | 2.049(3) | Ni4−O3 | 2.056(4) |
| Ni1−O4 | 2.061(3) | Ni4−O4 | 2.054(3) |
| Ni2−O1 | 2.047(3) | Ni1···Ni2 | 3.049(1) |
| Ni2−O2 | 2.052(4) | Ni2···Ni3 | 3.056(1) |
| Ni2−O4 | 2.055(3) | Ni1···Ni3 | 3.094(1) |
| Ni3−O1 | 2.064(4) | Ni2···Ni4 | 3.107(1) |
| Ni3−O2 | 2.055(3) | Ni1···Ni4 | 3.064(1) |
| Ni3−O3 | 2.041(3) | Ni3···Ni4 | 3.060(1) |
| Ni3−O1−Ni4 | 95.9(1) | Ni3−O1−Ni2 | 96.0(1) |
| Ni4−O1−Ni2 | 98.4(1) | Ni3−O2−Ni2 | 96.2(1) |
| Ni3−O2−Ni1 | 98.0(1) | Ni2−O2−Ni1 | 96.2(1) |
| Ni4−O3−Ni1 | 96.6(1) | Ni4−O3−Ni3 | 96.6(1) |
| Ni1−O3−Ni3 | 98.3(1) | Ni1−O4−Ni2 | 95.6(1) |
| Ni1−O4−Ni4 | 96.3(1) | Ni2−O4−Ni4 | 98.3(1) |

$[Ni_7(OH)_8(hfac)_6(py)_6]·py$ **(2·py).** The cluster (Figure 2a) crystallizes in the monoclinic $P2_1/n$ space group. The central nickel ion is located on a $2a$ special Wyckoff position and shared by two cubane moieties where the nickel(II) ions are connected by four hydroxo oxygen atoms to form a $\{Ni_4O_4\}$ cubane core (Figure 2b,c). The coordination spheres of the nickel(II) ions located on general positions are completed by one deprotonated hfac ligand and one pyridine molecule to form a $\{NO_5\}$ octahedral environment. The coordination environment of the central nickel(II) ion is completed by the symmetry operations of the space group, which is then an

**Figure 2.** (a) Molecular structure of $[\mathbf{Ni_7}]$ (**2**). (b) View of the asymmetric unit with the metal environment. (c) View showing $[\mathbf{Ni_7}]$ as the "condensation" of two $[\mathbf{Ni_4}]$ clusters sharing one metal ion. Hydrogen atoms have been omitted for clarity in (a) and (b).

octahedral coordination sphere made up of six oxygen atoms belonging to the hydroxyl groups (Figure 2b).

The $\{Ni_4O_4\}$ cores are more distorted than in the $[\mathbf{Ni_4}]$ precursor, as the Ni−O−Ni and the O−Ni−O angles vary from 95.8 to 100.4° and from 81.0 to 97.7°, respectively. Moreover, the coordination octahedra of the nickel(II) atoms are less regular than those in the precursor, except for the central nickel(II) ion, for which O−Ni−O angles deviate from 90° by less than 8° and the Ni−O bond lengths vary by less than 0.005 Å from the mean value of 2.045 Å. Concerning the external metal ion centers, the Ni−O bond lengths are slightly longer when the oxygen atom belongs to a hfac ligand (2.075 Å) in comparison with the oxygen atoms belonging to a $\mu_3$-OH group (2.043 Å). In addition, the Ni−N(pyridine) bond lengths are the longest ones (∼2.097 Å). The O−Ni−O and O−Ni−N angles deviate from 90° by 10°. It should be noted that Ni−O(hfac) bond lengths are longer in the $[\mathbf{Ni_7}]$ (**2**) cluster (2.075 Å for the external Ni ions) than in the $[\mathbf{Ni_4}]$ (**1**) cubane (2.051 Å), whereas the Ni−$\mu_3$-OX bond lengths are almost equal in $[\mathbf{Ni_7}]$ (X = H, 2.045 Å) and in $[\mathbf{Ni_4}]$ (X = CH₃, 2.053 Å). For the Ni···Ni distances, the slight distortion of the $\{Ni_4\}$ cubane core induces shorter distances between the central position and

the external positions (3.043 Å) than between external positions (3.107 Å) (Table 3).

**Table 3. Selected Bond Lengths (Å), Distances (Å), and Angles (deg) for 2**

| | | | |
|---|---|---|---|
| Ni1−O83 | 2.055(5) (×2) | Ni4−O81 | 2.053(6) |
| Ni1−O82 | 2.048(6) (×2) | Ni4−O83 | 2.030(6) |
| Ni1−O84 | 2.043(6) (×2) | Ni4−O84 | 2.033(5) |
| Ni2−O81 | 2.063(6) | Ni1···Ni2 | 3.057(1) |
| Ni2−O82 | 2.031(6) | Ni1···Ni3 | 3.040(1) |
| Ni2−O83 | 2.035(6) | Ni1···Ni4 | 3.034(1) |
| Ni3−O81 | 2.086(5) | Ni2···Ni4 | 3.098(2) |
| Ni3−O82 | 2.022(6) | Ni2···Ni3 | 3.119(2) |
| Ni3−O84 | 2.030(6) | Ni3···Ni4 | 3.105(2) |
| Ni3−O81−Ni2 | 97.5(2) | Ni3−O81−Ni4 | 97.2(2) |
| Ni2−O81−Ni4 | 97.6(2) | Ni1−O82−Ni2 | 97.1(2) |
| Ni1−O82−Ni3 | 96.6(2) | Ni2−O82−Ni3 | 100.6(2) |
| Ni1−O83−Ni2 | 96.7(2) | Ni1−O83−Ni4 | 95.9(2) |
| Ni2−O83−Ni4 | 99.3(3) | Ni1−O84−Ni4 | 96.2(2) |
| Ni1−O84−Ni3 | 96.6(2) | Ni4−O84−Ni3 | 99.7(2) |

The shortest distance between the nickel ions of two clusters is 12.075 Å. While the unit cell is completed by two crystallization disordered pyridine molecules (67% and 33%), only hydrogen bonds are found between the $[\mathbf{Ni_7}]$ clusters. Thus, it is presumed that the neutral entities are well isolated from each other and that the structural cohesion can be ascribed to weak interactions.

**dc SQUID Magnetometry.** *$[Ni_4(OCH_3)_4(hfac)_4(CH_3OH)_4]$ (1).* The thermal variation of $\chi T$ is shown in Figure 3. At room
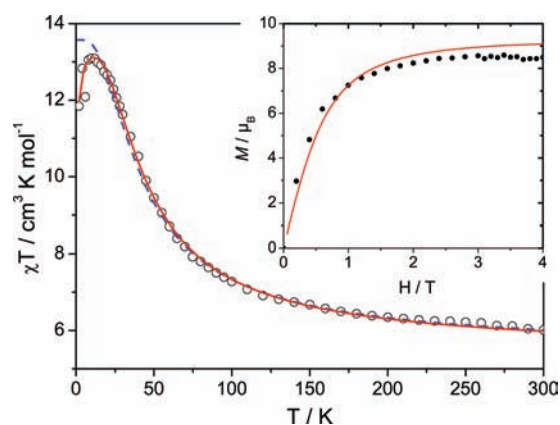


**Figure 3.** Thermal dependence of the $\chi T$ product of $[\mathbf{Ni_4}]$ (**1**). The blue dashed line shows the fit according to eq 1 and the red line for the fit including intermolecular interactions. The inset reports the magnetization curve at 2 K and the Brillouin curve for S = 4.

temperature, the $\chi T$ product of 5.97 cm³ K mol⁻¹ is higher than the expected value for four uncorrelated Ni(II) ions with g = 2 (4 cm³ K mol⁻¹). Upon cooling, $\chi T$ continuously increases and reaches a maximum of 13.10 cm³ K mol⁻¹ at 10 K, close to the expected value for an S = 4 ground state with a g value of 2.29. This feature indicates dominant intracluster ferromagnetic interactions. Below 10 K, the $\chi T$ product slowly decreases, probably due to weak intermolecular antiferromagnetic interactions and/or small anisotropy. The magnetization curve recorded at 2 K is reported in the inset of Figure 3. It shows a continuous increase up to the saturation value of 8.45 $\mu_B$, which corresponds well to a ground-state spin S = 4, in

agreement with the $\chi T$ data. However, this magnetization curve cannot be nicely fitted by a Brillouin equation for $S = 4$, probably due to the presence of intermolecular interaction and/or anisotropy.

This magnetic behavior, as well as the crystal structure, are very similar to those observed in the nonfluorinated analogue and other nickel(II) cubanes.[20]

Therefore, the data were analyzed using two different coupling constants $J_1$ and $J_2$, expressed in the spin Hamiltonian of eq 1, in agreement with the presence of two long Ni···Ni

$$\hat{H} = -2J_1(\hat{S}_{Ni1}\hat{S}_{Ni4} + \hat{S}_{Ni1}\hat{S}_{Ni3} + \hat{S}_{Ni2}\hat{S}_{Ni4} + \hat{S}_{Ni2}\hat{S}_{Ni3})$$
$$- 2J_2(\hat{S}_{Ni1}\hat{S}_{Ni2} + \hat{S}_{Ni3}\hat{S}_{Ni4}) \qquad (1)$$

distances ($\sim$3.10 Å) associated with nearly $98.2 \pm 0.2°$ Ni−O−Ni angles and four short Ni···Ni distances ($\sim$ 3.05 Å) associated with nearly $96.2 \pm 0.4°$ Ni−O−Ni angles (Table 2). The fit process, considering only two intramolecular couplings, leads to $J_1 = +9.2$ cm$^{-1}$ and $J_2 = +4.0$ cm$^{-1}$ with $g = 2.32$, which agrees with the differences in Ni···Ni distances and Ni−O−Ni angles (Figure 3). However, as expected, this set of parameters does not allow reproducing the low-temperature decrease of $\chi T$. This is only achieved when taking into account an intercluster interaction ($zJ' = -0.013$ cm$^{-1}$) but the effect is to make $J_1$ and $J_2$ equal with a medium value of 5.5 cm$^{-1}$. This value is close to 7 cm$^{-1}$, which was reported for the nonfluorinated cubane analogue.[20] Whereas it is difficult to choose between both sets of fitting parameters, they both clearly indicate strong ferromagnetic interactions. The difficulty in fitting the low-temperature region may be mostly due to magnetic anisotropy, as low-temperature values are dependent on the magnetic field. This has recently been exemplified for another $[Ni_4]$ complex.[52]

*[Ni₇(OH)₈(hfac)₆(py)₆]·py (2·py).* The thermal variation of $\chi T$ is shown in Figure 4. At room temperature, the $\chi T$ product of 9.06 cm$^3$ K mol$^{-1}$ is slightly higher than the expected value for seven uncorrelated Ni(II) ions with $g = 2$ (8 cm$^3$ K mol$^{-1}$). Upon cooling, $\chi T$ continuously increases and reaches a maximum of 28.43 cm$^3$ K mol$^{-1}$ at 5 K. As for $[Ni_4]$ (**1**), this feature indicates dominant intracluster ferromagnetic interactions. Below 5 K, the $\chi T$ product slowly decreases,
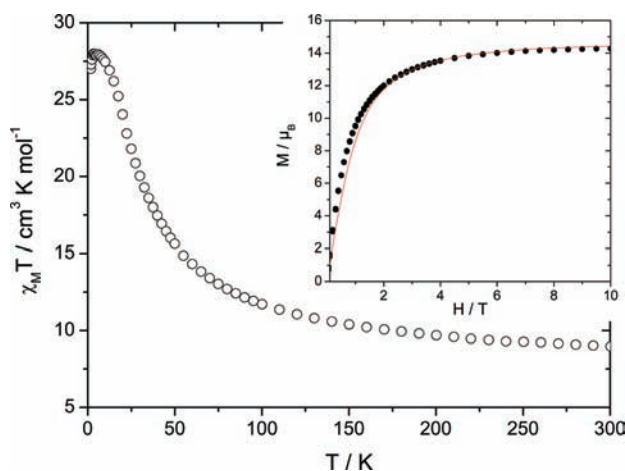


**Figure 4.** Thermal dependence of the $\chi T$ product of $[Ni_7]$ (**2**). The inset reports the magnetization curve at 5 K and the Brillouin curve for $S = 7$.

probably due to weak intermolecular antiferromagnetic interactions and/or small anisotropy. The magnetization curve recorded at 5 K is reported in the inset of Figure 4. It shows a continuous increase up to saturation at 14.33 $\mu_B$ for an applied magnetic field of 10 T. This curve differs only slightly and at low field from a Brillouin function for an $S = 7$ ground state. Plots of the reduced magnetization for different temperatures (3, 5, 18 K) are given in the Supporting Information (Figure 1S) and show only small differences, characteristic of a small magnetic anisotropy.

We used the Magpack program to simulate both $\chi T$ and $M$ curves.[65,66] The number of exchange interaction pathways is important, up to 12. However, from the crystal structure it may be seen that the $[\mathbf{Ni7}]$ molecules are centrosymmetric at the central nickel(II) Ni1. Moreover, a detailed analysis of the structural parameters within the asymmetric moiety $[Ni1Ni2\text{-}Ni3Ni4]$ shows that Ni···Ni distances between the central Ni1 and Ni2, Ni3, and Ni4 are shorter ($3.034(1)-3.057(1)$ Å) than those between the external ions Ni2, Ni3, and Ni4 ($3.098(2)-3.119(2)$ Å). These distances are also associated with different Ni−O−Ni angles. The bonds involving the central nickel Ni1 show a mean angle value of 96.5° with a variation of 0.4°, while those concerning the external nickel ions only are around 98.4° with a variation of 1.7°. Therefore, we took into account the two different exchange parameters $J_3$ and $J_4$ according to the Hamiltonian given by eq 2, where $J_3$ describes the interaction between the central and the external nickel ions and $J_4$ describes the interaction between the external ions.

$$\hat{H} = -2J_3(\hat{S}_{Ni1}\hat{S}_{Ni2} + \hat{S}_{Ni1}\hat{S}_{Ni3} + \hat{S}_{Ni1}\hat{S}_{Ni4} + \hat{S}_{Ni1}\hat{S}_{Ni2'}$$
$$+ \hat{S}_{Ni1}\hat{S}_{Ni3'} + \hat{S}_{Ni1}\hat{S}_{Ni4'}) - 2J_4(\hat{S}_{Ni2}\hat{S}_{Ni3} + \hat{S}_{Ni3}\hat{S}_{Ni4}$$
$$+ \hat{S}_{Ni2}\hat{S}_{Ni4} + \hat{S}_{Ni2}\hat{S}_{Ni3'} + \hat{S}_{Ni3}\hat{S}_{Ni4'} + \hat{S}_{Ni2}\hat{S}_{Ni4'}) \qquad (2)$$

As in the cubane precursor $[\mathbf{Ni_4}]$ (**1**), the extraction of a clear set of parameters is tricky. According to the structural similitudes, a simulation was performed using the exchange constants obtained for **1**. However, none of the set of parameters tested can nicely reproduce the maximum in the $\chi T$ curve, even considering intracluster antiferromagnetic interactions. Even the introduction of intermolecular interactions failed to reproduce the experimental curve. Therefore, this maximum does not only come from intermolecular interactions but also from anisotropic effects, which have to be clarified. In addition, the presence of such anisotropy induces a dependence of the $\chi T$ maximum value on the field applied for the measurement, making the estimation of the ground spin state difficult, as pointed out for **1**.[52] We therefore performed high-field electron paramagnetic resonance to identify the spin ground state and the anisotropy of **2**.

**High-Frequency Electron Paramagnetic Resonance.** HF-EPR proved to be a very powerful method in determining spin Hamiltonian parameters of molecular nanomagnets when the ground spin state is well isolated from the excited states.[67−71] One of the main advantages of this technique is the simplification of the spectra induced by high fields, when ZFS terms can be treated, in a first approximation, as a perturbation of the Zeeman interaction. As a consequence, the $D$ value of a purely axial system can be obtained by simple inspection of the spectrum, as successive transitions are separated by $2D/(g_\parallel\mu_B)$ in the parallel region and by $D/$

($g_\perp \mu_B$) in the perpendicular direction. Furthermore, the Boltzmann effect allows obtaining the sign of the ZFS at low temperature: a negative $D$ value will enhance the intensity of the parallel transitions appearing in the low-field part of the spectrum, while the opposite will be observed for a complex with a positive $D$ value.

In the case of $[Ni_4]$ (**1**), the powder spectra recorded at 190 GHz show a structured signal, whereas at 285 GHz only the 20 K spectrum presents some visible structure (Figure 5). At both
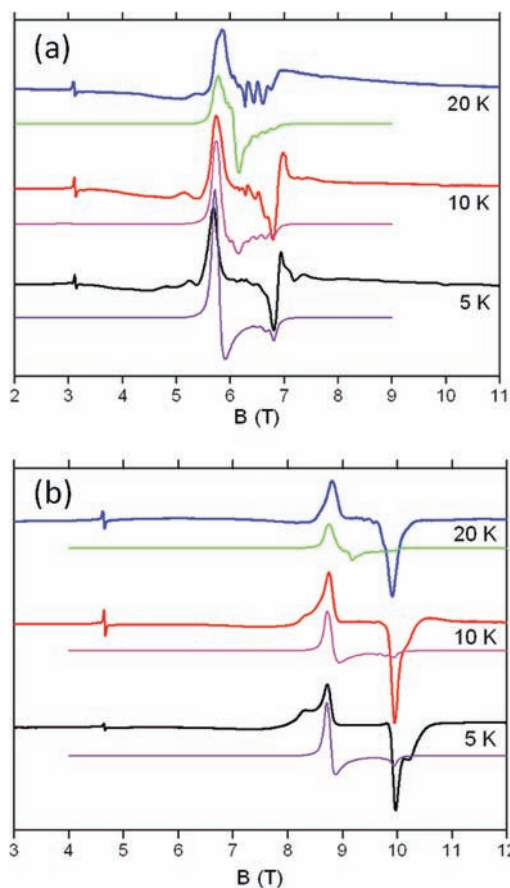


**Figure 5.** EPR powder spectra for $[Ni_4]$ (**1**) recorded at (a) 190 GHz and (b) 285 GHz at 5 K, 10 K, and 20 K (bottom to top). The black, red, and blue lines denote the experimental spectra, whereas the violet, pink, and green lines are calculated spectra, with the parameters given in the text.

frequencies, the spectra extend over about 1.5 T in the $g = 2$ region together with a "forbidden" transition at half-field. At 190 GHz, it is possible to reproduce the recorded spectra, at least as far as the positions of the signals are concerned, with the following parameters for an $S = 4$ spin Hamiltonian: $D = +0.08$ cm$^{-1}$, $E = 0.004$ cm$^{-1}$, $g_x = g_y = 2.26$, and $g_z = 2.17$. The simulated spectra also present a half-field signal, but it looks much weaker than in the experimental spectra, perhaps because of a broader line width. These parameters also give a reasonable picture of the spectrum obtained at 285 GHz and 5 K. However, the higher temperature spectra are not so well accounted for, as the two main signals, observed at 8.7 and 10 T, remain roughly unchanged when the temperature is increased, with only tiny structures visible below 10 T at 10 and 20 K, conversely to what is expected for a simple $S = 4$ spin. Only the outer shoulders of these main signals are

changing clearly with temperature, but they have no clear equivalents in the 190 GHz spectra. This can be the result of the presence of excited spin states close in energy to the ground spin state.

For $[Ni_7]$ (**2**), an even more complex picture is found from the EPR study. The powder spectra recorded at 5 K and four different frequencies ranging between 190 and 345 GHz are presented in Figure 6b. For the three lower frequencies, the
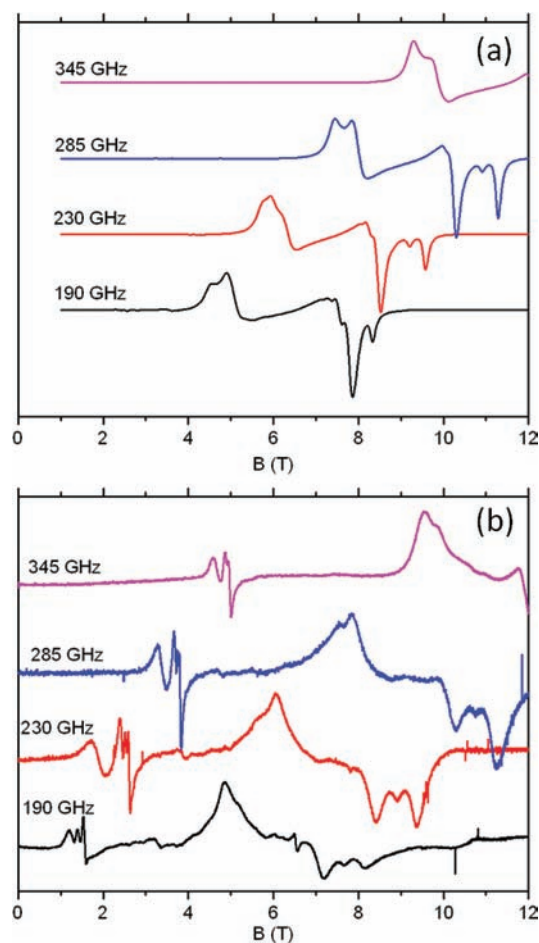


**Figure 6.** Powder EPR spectra for $[Ni_7]$ (**2**) at 5 K and several frequencies (indicated on the figure): (a) calculated spectra obtained considering an $S = 6$ ground multiplet and an $S = 7$ first excited multiplet, with the parameters given in the text and an energy gap of 9 cm$^{-1}$ between the two states; (b) experimental spectra recorded on a pellet.

main signal extends over ~4 T around $g = 2$ (at 345 GHz only the low-field part of this signal is observed as $g = 2$ corresponds to 12.3 T) together with forbidden transitions at lower magnetic fields. The spectra obtained at 285 GHz in the temperature range from 5 to 20 K are shown in Figure 7b. At this frequency, the main signal extends roughly from 7 to 11 T. When the temperature is increased to 10 and 20 K, regular structures appear which are the signature of the presence of a small ZFS associated with a spin value larger than the $S = 1$ single ion spin (Figure 7b). The picture emerging from the multifrequency measurements is that, at least, one excited spin level $S''$ is very close in energy to the ground spin state $S$. Furthermore, this excited level has a larger spin value than for the ground state. Indeed, at 5 K, rather weak signals present on the extremes of the main signal at low frequencies are getting
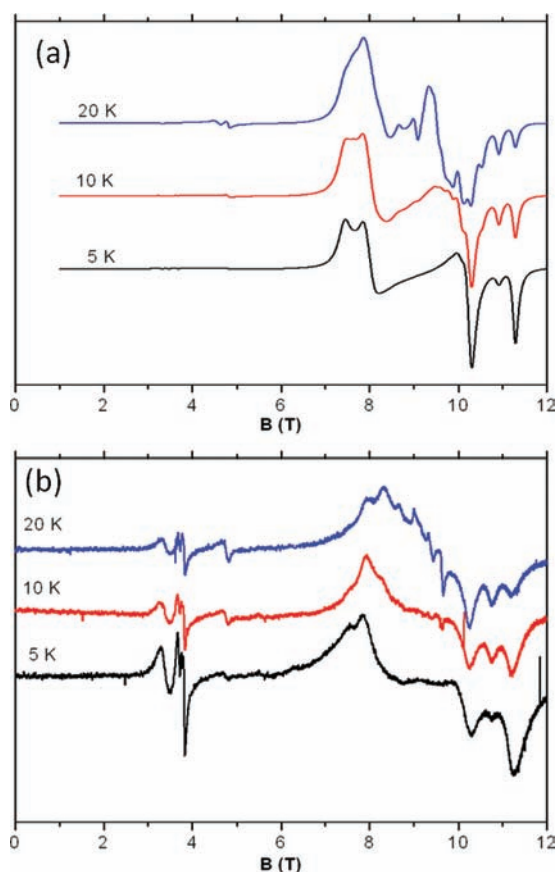
**Figure 7.** Powder EPR spectra for [Ni₇] (2) at 285 GHz and several temperatures (indicated on the figure): (a) calculated spectra obtained considering an $S = 6$ ground multiplet and an $S = 7$ first excited multiplet, with the parameters given in the text and an energy gap of 9 cm$^{-1}$ between the two states; (b) experimental spectra recorded on a pellet.

more and more intense when the frequency and thus the resonant magnetic field are increased (Figure 6b). On the high-field side of the main signal, a weak signal is observed at 5 K and 190 GHz (at 8.1 T), in comparison to the other high-field transition observed at 7.2 T; this initially weak signal gains intensity with an increase of the resonance field, to be comparable to the other high-field transition at 230 GHz (signals at 8.4 and 9.4 T, respectively) and even to become the most intense high-field signal at 285 GHz (signal at 11.2 T compared to that at 10.2 T). Similarly, on the low-field side of the main signal at 5 K and 190 GHz, a very weak shoulder is observed at 4.1 T with respect to the first signal at 4.8 T. This shoulder increases at 230 GHz (found at 5.6 T with respect to the first signal at 6.0 T) and even more at 285 GHz (signals at 7.5 and 7.8 T) to become the most intense signal at 345 GHz (signals at 9.5 and 9.8 T). This indicates that the $M' = -S'$ level of the excited $S'$ spin multiplet becomes lower in energy than the $M = -S$ level of the ground $S$ multiplet in a field region close to 9 T, which means that the energy difference between these two levels is about 9−10 cm$^{-1}$, with the hypothesis that $S' = S + 1$.

As a result, the observed spectra represent a superposition of contributions from at least two spin multiplets, with the further problem that, EPR spectra being recorded by varying the applied magnetic field, the relative weights of these contributions are not constant over each spectrum. Thus, it is

hard to ascribe with certainty the structure seen at 10 or 20 K and to use it to determine the magnetic anisotropy of the lowest spin state(s). An estimate of the magnetic anisotropy can be made relying on the position of the extreme lines, for the lowest multiplets, depending on the spin value of this multiplet. As an excited multiplet has a larger spin value, the maximum possible value for the ground state is $S = 6$. As this is also the ground state expected on the basis of magnetic susceptibility measurements, the analysis of the EPR spectra will be done considering an $S = 6$ ground state with a first excited $S = 7$ state. At 190 GHz and 5 K, only two signals (one at 4.8 T and the other at 7 T) arise from the ground state, indicating a negligible rhombic anisotropy. One obtains the following values for $S = 6$: $D_6 = -0.18$ cm$^{-1}$ ($E_6 = 0$ cm$^{-1}$) with $g_{\parallel} = 2.05$ and $g_{\perp} = 2.20$. For the excited multiplet, it is not possible to estimate the rhombicity from a simple inspection of the spectrum, due to the presence of the signals arising from the ground multiplet. Considering an $S = 7$ excited state, and making the simplifying assumption of an isotropic $g$ value, a reasonable reproduction of the signals (especially the extreme ones) is obtained with the following parameters: $D_7 = 0.20$ cm$^{-1}$, $E_7 = 0.015$ cm$^{-1}$ ($g_{\parallel} = g_{\perp} = 2.3$). Calculated spectra, considering these two multiplets and introducing a zero field energy gap of 9 cm$^{-1}$ between them, are shown in Figures 6a (several frequencies and 5 K) and 7a (several temperatures and 285 GHz). At 5 K, the comparison of calculated and measured spectra (Figure 6) at different frequencies shows that the picture of an excited multiplet with a larger spin value than the ground multiplet indeed reproduces the trend of the external signals to gain intensity with an increase of frequency (and thus of magnetic field) with respect to the more central lines. Furthermore, as shown in Figure 7, the evolution of the spectra with temperature is also reasonably reproduced. However, with such a complex pattern and so many adjustable parameters, a real fitting of the spectra is not possible and the values of the parameters should be rather considered as reasonable estimates.

Unfortunately for this complex, even with the multifrequency study, it is not possible to determine precisely the magnetic anisotropy of the ground spin state due to the presence of at least one excited spin multiplet very close in energy. Furthermore, the spin ground state cannot be completely ascertained, even if an $S = 6$ ground state (with a negative ZFS $D \approx -0.18$ cm$^{-1}$) appears highly probable.

**Micro-SQUID Magnetometry.** The presence of high-spin ground-state values for [Ni₄] (1) and [Ni₇] (2) clusters associated with important anisotropy constants determined by EPR spectroscopy led us to study their magnetic behavior at very low temperatures, looking for the possible occurrence of single-molecule magnet behavior in [Ni₇]. Therefore, a low-temperature study of the hysteresis loops was performed down to 40 mK with an array of micro-SQUIDs.[11] For [Ni₄], the temperature dependence of the magnetization down to 0.04 K did not show any hysteresis loop (Figure 8). However, the "double-S-like" curve is characteristic of antiferromagnetic intermolecular interactions between the clusters, which agrees with our assumptions from the dc magnetic measurements. For [Ni₇] (2) smooth hysteresis loops appear below 0.5 K with coercivities which increase upon cooling to reach 200 Oe at 40 mK (Figure 9a) and with increasing sweep rate (Figure 9b). This behavior indicates with no doubt an SMM behavior for [Ni₇]. No step characteristic of quantum tunneling of the magnetization (QTM) was observed which may be due to step broadening from the low-lying excited state.
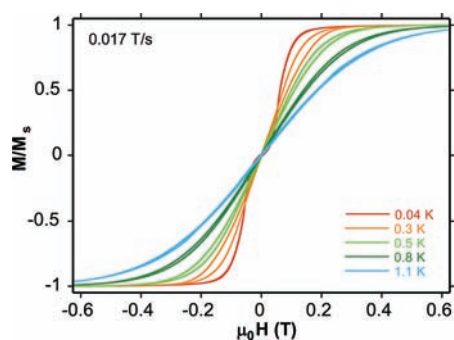
**Figure 8.** Plots of normalized magnetization ($M/M_s$) versus applied field ($\mu_0 H$) for $[Ni_4]$ (**1**). The loops are shown at different temperatures at 0.017 T/s$^{-1}$.
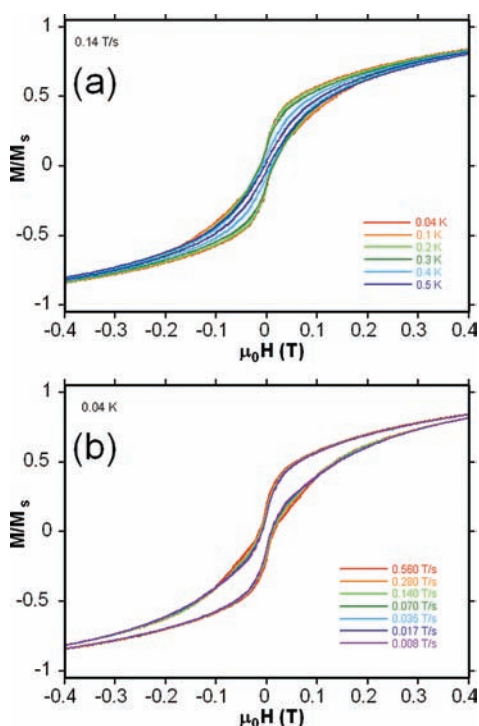


**Figure 9.** Plots of normalized magnetization ($M/M_s$) versus applied field ($\mu_0 H$) for $[Ni_7]$ (**2**): (a) at sweep rate 0.14 T/s$^{-1}$ and the indicated temperatures; (b) at 0.04 K and indicated sweep rates.

## CONCLUSIONS

In this paper we report the synthesis, crystal structures, and magnetic and EPR properties of tetranuclear $[Ni_4]$ and heptanuclear $[Ni_7]$ nickel(II) complexes. The heptanuclear complex $[Ni_7]$ was synthesized using the tetranuclear complex $[Ni_4]$ as a precursor and may be viewed as the condensation of two $[Ni_4]$ groups sharing one nickel(II) ion. The magnetic studies show for both complexes dominant ferromagnetic interactions between the nickel(II) ions, in agreement with structural features. For the tetranuclear complex $[Ni_4]$ this gives an $S = 4$ ground-state spin which is clearly confirmed by the high-frequency EPR study. For the heptanuclear complex $[Ni_7]$ the ground-state spin stays undetermined despite many efforts. The answer is partially determined by the high-frequency EPR study, which shows that an excited state with a larger spin value lies very close in energy to the ground spin state. The EPR study enables us to determine that the ground spin state is not the $S = 7$ that would be expected but $S < 7$ and most probably $S$

$= 6$. A lower spin ground state seems to be excluded, in agreement with structural features that favor ferromagnetic interactions between all nickel(II) ions. However, modeling a ground $S = 6$ spin state from the magnetic structure of the molecule is not obvious. $S = 7$ could be obtained considering ferromagnetic interactions between all the Ni(II) ions, whereas an $S = 5$ ground state, excluded here, could follow from a dominant antiferromagnetic exchange between the central ion and the external ions, but there is no simple single ion spin arrangement leading to $S = 6$. Thus, it is difficult to propose a reasonable fitting of the $\chi T$ curve. Moreover, the presence of negative $D$ values ($<-0.15$ cm$^{-1}$) indicates that the dc magnetic measurements are field-dependent, which contributes to the difficulties encountered in the fitting process of the $\chi T$ curve.

Very low temperature studies show that only the heptanuclear complex behaves like an SMM, in agreement with the EPR study that found a negative axial anisotropy for $[Ni_7]$ but a positive axial term for $[Ni_4]$. The synthesis process may seem complicated, but it is reproducible and works for other metal ions. Thus, starting from the tetranuclear cobalt analogue $[Co_4]$, it was possible to obtain the cobalt heptanuclear analogue $[Co_7]$, which will be reported later.

## ■ ASSOCIATED CONTENT

### ⓢ Supporting Information

Reduced magnetization data for **2** at 1.8, 3, and 5 K (Figure 1S) and CIF files giving crystallographic refinement details for **1** and **2**. This material is available free of charge via the Internet at http://pubs.acs.org.

## ■ AUTHOR INFORMATION

### Corresponding Author
*E-mail: luneau@univ-lyon1.fr.

### Present Address
∥CNRS, Université de Bordeaux, ICMCB, 87 avenue du Dr. A. Schweitzer, F-33608 Pessac, France.

### Notes
The authors declare no competing financial interest.

## ■ DEDICATION

Dedicated to Hubert Le Bozec on the occasion of his 60th birthday.

## ■ REFERENCES

(1) Caneschi, A.; Gatteschi, D.; Sessoli, R.; Barra, A.-L.; Brunel, L. C.; Guillot, M. *J. Am. Chem. Soc.* **1991**, *113*, 5873−5874.
(2) Sessoli, R.; Gatteschi, D.; Caneschi, A.; Novak, M. *Nature* **1993**, *365*, 141−143.
(3) Sessoli, R.; Tsai, H.-L.; Schake, A. R.; Wang, S.; Vincent, J. B.; Folting, K.; Gatteschi, D.; Christou, G.; Hendrickson, D. N. *J. Am. Chem. Soc.* **1993**, *115*, 1804−1816.
(4) Gatteschi, D.; Caneschi, A.; Pardi, L.; Sessoli, R. *Science* **1994**, *265*, 1054−1058.
(5) Gatteschi, D.; Sessoli, R. *Angew. Chem. Int. Ed* **2003**, *42*, 268−297.

(6) Christou, G.; Gatteschi, D.; Hendrickson, D. N.; Sessoli, R. *MRS Bull.* **2000**, *25* (11), 66−71.

(7) Ritter, S. K. *Chem. Eng. News* **2004**, *82*, 29−32.

(8) Aromi, G.; Brechin, E. K. *Struct. Bonding (Berlin)* **2006**, *122*, 1−67.

(9) Chudnovsky, E., M. *Science* **1996**, *274*, 938−939.

(10) Leuenberger, M., N.; Loss, D. *Nature* **2001**, *410*, 789−793.

(11) Wernsdorfer, W. *Adv. Chem. Phys.* **2001**, *118*, 99−189.

(12) Gatteschi, D.; Sessoli, R.; Villain, J. *Molecular Nanomagnets*; Oxford University Press: London, 2006.

(13) Winpenny, R. E. P. *Adv. Inorg. Chem.* **2001**, *52*, 1−111.

(14) Christou, G. *Polyhedron* **2005**, *24*, 2065−2075.

(15) Sessoli, R.; Powell, A. K. *Coord. Chem. Rev.* **2009**, *253*, 2328−2341.

(16) Andruh, M.; Costes, J. P.; Diaz, C.; Gao, S. *Inorg. Chem.* **2009**, *48*, 3342−3359.

(17) Ababei, R.; Li, Y. G.; Roubeau, O.; Kalisz, M.; Brefuel, N.; Coulon, C.; Harte, E.; Liu, X. T.; Mathoniere, C.; Clerac, R. *New J. Chem.* **2009**, *33*, 1237−1248.

(18) Rinehart, J. D.; Fang, M.; Evans, W. J.; Long, J. *Nat. Chem.* **2011**, *3*, 538−542.

(19) Mills, D. P.; Moro, F.; McMaster, J.; van Slageren, J.; Lewis, W.; Blake, A. J.; Liddle, S. T. *Nat. Chem.* **2011**, *3*, 454−460.

(20) Bertrand, J. A.; Ginsberg, A. P.; Kaplan, R. I.; Kirkwood, C. E.; Martin, R. L.; Sherwood, C. *Inorg. Chem.* **1971**, *10*, 240−246.

(21) Jones, W. J.; Gupta, S.; Theriot, L. J.; Helm, F. T.; Baker, W. A. *Inorg. Chem.* **1978**, *17*, 87−90.

(22) Merz, L.; Haase, W. *Z. Naturforsch.* **1976**, *31a*, 177−182.

(23) Oshio, H.; Nihei, M.; Koizumi, S.; Shiga, T.; Nojiri, H.; Nakano, M.; Shirakawa, N.; Akatsu, M. *J. Am. Chem. Soc.* **2005**, *127*, 4568−4569.

(24) Oshio, H.; Hoshino, N.; Ito, T.; Nakano, M. *J. Am. Chem. Soc.* **2004**, *126*, 8805−8812.

(25) Schelter, E. J.; Prosvirin, A. V.; Dunbar, K. R. *J. Am. Chem. Soc.* **2004**, *126*, 15004−15005.

(26) Schelter, E. J.; Karadas, F.; Avendano, C.; Prosvirin, A. V.; Wernsdorfer, W.; Dunbar, K. R. *J. Am. Chem. Soc.* **2007**, *129*, 8139−8149.

(27) Bertrand, J. A.; Kelley, J. A. *Inorg. Chim. Acta* **1970**, *4*, 203−209.

(28) Halcrow, M. A.; Sun, J.-S.; Huffman, J. C.; Christou, G. *Inorg. Chem.* **1995**, *34*, 4167−4177.

(29) Tercero, J.; Ruiz, E.; Alvarez, S.; Rodríguez-Fortea, A.; Alemany, P. *J. Mater. Chem.* **2006**, *16*, 2729−2735.

(30) Oshio, H.; Hoshino, N.; Ito, T. *J. Am. Chem. Soc.* **2000**, *122*, 12602−12603.

(31) Ribas-Arino, J.; Baruah, T.; Pederson, M. R. *J. Am. Chem. Soc.* **2006**, *128*, 9497−9505.

(32) Nakano, M.; Oshio, H. *Chem. Soc. Rev.* **2011**, *40*, 3239−3248.

(33) Aronica, C.; Pilet, G.; Chastanet, G.; Wernsdorfer, W.; Jacquot, J.-F.; Luneau, D. *Angew. Chem., Int. Ed.* **2006**, *45*, 4659−4662.

(34) Aronica, C.; Chastanet, G.; Pilet, G.; Le Guennic, B.; Robert, V.; Wernsdorfer, W.; Luneau, D. *Inorg. Chem.* **2007**, *46*, 6108−6119.

(35) Aronica, C.; Chumakov, Y.; Jeanneau, E; Luneau, D.; Neugebauer, P.; Barra, A.-L.; Gillon, B. G., A.; Cousson, A.; Tercero, J.; Ruiz, E. *Chem. Eur. J.* **2008**, *14*, 9540−9548.

(36) Chibotaru, L. F.; Ungur, L.; Aronica, C.; Elmoll, H.; Pilet, G.; Luneau, D. *J. Am. Chem. Soc.* **2008**, *130*, 12445−12455.

(37) Milios, C. J.; Vinslava, A.; Wernsdorfer, W.; Moggach, S.; Parsons, S.; Perlepes, S. P.; Christou, G.; Brechin, E. K. *J. Am. Chem. Soc.* **2007**, *129*, 2754−2755.

(38) Milios, C. J.; Inglis, R.; Vinslava, A.; Bagai, R.; Wernsdorfer, W.; Parsons, S.; Perlepes, S. P.; Christou, G.; Brechin, E. K. *J. Am. Chem. Soc.* **2007**, *129*, 12505−12511.

(39) Taguchi, T.; Wernsdorfer, W.; Abboud, K. A.; Christou, G. *Inorg. Chem.* **2010**, *49*, 10579−10589.

(40) Alexandropoulos, D. I.; Papatriantafyllopoulou, C.; Aromi, G.; Roubeau, O.; Teat, S. J.; Perlepes, S. P.; Christou, G.; Stamatatos, T. C. *Inorg. Chem.* **2010**, *49*, 3962−3964.

(41) Cadiou, C.; Murrie, M.; Paulsen, C.; Villar, V.; Wernsdorfer, W.; Winpenny, R. E. P. *Chem. Commun.* **2001**, 2666−2667.

(42) Wernsdorfer, W.; Aliaga-Alcade, N.; Hendrickson, D. N.; Christou, G. *Nature* **2002**, *416*, 406−409.

(43) Andres, H.; Basler, R.; Blake, A. J.; Cadiou, C.; Chaboussant, G.; Grant, C. M. G.; Güdel, H.-U.; Murrie, M.; Parsons, S.; Paulsen, C.; Semadini, F.; Villar, V.; Wernsdorfer, W.; Winpenny, R. E. P. *Chem. Eur. J.* **2002**, *8*, 4867−4876.

(44) Ochsenbein, S. T.; Murrie, M.; Rusanov, E.; Stoeckli-Evans, H.; Sekine, C.; Güdel, H.-U. *Inorg. Chem.* **2002**, 5133−5140.

(45) Yang, E.-C.; Wernsdorfer, W.; Hill, S.; Edwards, R. S.; Nakano, M.; Maccagnano, S.; Zakharov, L. N.; Rheingold, A. L.; Christou, G.; Hendrickson, D. N. *Polyhedron* **2003**, *22*, 1727−1733.

(46) Moragues-Canovas, M.; Helliwell, M.; Ricard, L.; Rivière, E.; Wernsdorfer, W.; Brechin, E.; Mallah, T. *Eur. J. Inorg. Chem.* **2004**, 2219−2222.

(47) Bell, A.; Aromi, G.; Teat, S. J.; Wernsdorfer, W.; Winpenny, R. E. P. *Chem. Commun.* **2005**, 2808−2810.

(48) Aromi, G.; Parsons, S.; Wernsdorfer, W.; Brechin, E. K.; McInnes, E. J. L. *Chem. Commun.* **2005**, 5038−5040.

(49) Aromi, G.; Bouwman, E.; Burzuri, E.; Carbonera, C.; Krzystek, J.; Luis, F.; Schlegel, C.; van Slageren, J.; Tanase, S.; Teat, S. J. *Chem. Eur. J.* **2008**, *14*, 11158−11166.

(50) Bouldalis, A. K.; Pissas, M.; Raptopoulou, C. P.; Psycharis, V.; Abarca, B.; Ballesteros, R. *Inorg. Chem.* **2008**, *47*, 10674−10681.

(51) Ferguson, A.; Lawrence, J.; Parkin, A.; Sanchez-Benitez, J.; Kamenev, K. V.; Brechin, E. K.; Wernsdorfer, W.; Hill, S.; Murrie, M. *Dalton Trans.* **2008**, 6409−6414.

(52) Serna, Z.; De la Pinta, N.; Urtiaga, M. K.; Lezama, L.; Madariaga, G.; Clemente-Juan, J. M.; Coronado, E.; Cortes, R. *Inorg. Chem.* **2010**, *49*, 11541−11549.

(53) Ferguson, A.; Schmidtmann, M.; Brechin, E. K.; Murrie, M. *Dalton Trans.* **2011**, *40*, 334−336.

(54) Zhang, S. H.; Li, N.; Ge, C. M.; Feng, C.; Ma, L. F. *Dalton Trans.* **2011**, *40*, 3000−3007.

(55) Nonius BV: Delft, The Netherlands, 1997−2001.

(56) Altomare, A.; Burla, M. C.; Camalli, M.; Cascarano, G. L.; Giacovazzo, C.; Guagliardi, A.; Moliterni, A. G. G.; Polidori, G.; Spagna, R. *J. Appl. Crystallogr.* **1999**, *32*, 115−119.

(57) Watkin, D. J., Prout, C. K., Carruthers, J. R., Betteridge, P. W. *CRISTAL Issue 11*; Chemical Crystallography Laboratory, Oxford, U.K., 1999.

(58) Wernsdorfer, W.; Chakov, N. E.; Christou, G. *Phys. Rev. B* **2004**, *70*, 132413.

(59) Jacobsen, C. J. H.; Pedersen, E.; Villadsen, J.; Weihe, H. *Inorg. Chem.* **1993**, *32*, 1216−1221.

(60) Aromi, G.; Gamez, P.; Reedijk, J. *Coord. Chem. Rev.* **2008**, *252*, 964−989.

(61) Vigatoa, P. A.; Peruzzoa, V.; Tamburini, S. *Coord. Chem. Rev.* **2009**, *253*, 1099−1201.

(62) Petit, S.; Baril-Robert, F.; Pilet, G.; Reber, C.; Luneau, D. *Dalton Trans.* **2009**, 6809−6815.

(63) Ballester, L.; Coronado, E.; Gutierrez, A.; Monge, A.; Perpinan, M. F.; Pinilla, E.; Rico, T. *Inorg. Chem.* **1992**, *31*, 2053−2056.

(64) El Fallah, M. S.; Rentschler, E.; Caneschi, A.; Sessoli, R.; Gatteschi, D. *Inorg. Chem.* **1996**, *35*, 3723−3724.

(65) Borras-Almenar, J. J.; Clemente-Juan, J. M.; Coronado, E.; Tsukerblat, B. S. *Inorg. Chem.* **1999**, *38*, 6081−6088.

(66) Borras-Almenar, J. J.; Clemente-Juan, J. M.; Coronado, E.; Tsukerblat, B. S. *J. Comput. Chem.* **2001**, *22*, 985−991.

(67) Barra, A. L.; Gatteschi, D.; Sessoli, R. *Phys. Rev. B* **1997**, *56*, 8192−8198.

(68) Barra, A. L.; Gatteschi, D.; Sessoli, R. *Chem. Eur. J.* **2000**, *6*, 1608−1614.

(69) Hill, S.; Maccagnano, S.; Park, K.; Achey, R. M.; North, J. M.; Dalal, N. S. *Phys. Rev. B* **2002**, *65*, 224410.

(70) Kirman, C.; Lawrence, J.; Hill, S.; Yang, E. C.; Hendrickson, D. N. *J. Appl. Phys.* **2005**, *97*, 10M501.

(71) Takeda, K.; Awaga, K.; Inabe, T.; Yamaguchi, A.; Ishimoto, H.; Tomita, T.; Mitamura, H.; Goto, T.; Mori, N.; Nojiri, H. *Phys. Rev. B* **2002**, *65*, 094424.

6654

dx.doi.org/10.1021/ic3001637 | *Inorg. Chem.* 2012, 51, 6645−6654